Theor Chem Account (2008) 120:155–166
DOI 10.1007/s00214-007-0304-8

REGULAR ARTICLE

Ab initio molecular orbital study of the insertion of H_2 into POSS compounds

T. Kudo · M. Akasaka · M. S. Gordon

Received: 22 November 2006 / Accepted: 12 February 2007 / Published online: 10 May 2007

Abstract The insertion of one and two H_2 molecules into polyhedral oligomeric silsesquioxanes (POSS) was investigated as a function of the size of the cage, using both Hartree-Fock (HF) and second order perturbation theory (MP2) methods. Also investigated was the same reaction into the heavier groups 4 and 14 metal-substituted POSS (metallasilsesquioxanes) such as Ge-POSS, Si/Ge-mixed POSS, and Ti- and Zr-POSS. The properties of these species in comparison with those of POSS are discussed.

Keywords POSS · Silsesquioxanes · Insertion of H_2 · Molecular orbital

1 Introduction

For many years, polyhedral oligomeric silsesquioxanes (POSS), $[RSiO_{1.5}]_n$; $n = 4, 6, 8, 10, 12\ldots$, (usually referred to as T_n: see Scheme 1) have been the focus of considerable experimental and theoretical interest because of their wide variety of practical uses [1–4]. Interest in these compounds has focused on (1) the properties, mechanisms of formation and reactions of POSS and related compounds, including polymers [5–13], and (2) modeling catalytic reactions of POSS species on silica surfaces [14–20]. Various metals attached to incompletely condensed POSS compounds can play an important role in heterogeneous catalysis. However, the chemistry of fully or partially metal-substituted POSS is not well known, possibly because of experimental difficulties. However, such metallasilsesquioxanes may have the potential to be new functional materials or building blocks of useful polymers. Theoretical investigations of such compounds are expected to provide valuable insights into the chemistry of these species.

In the past several years, the authors have studied many aspects of POSS and related compounds. These investigations have included prediction and analysis of the mechanism of the formation of T_8, $[RSiO_{1.5}]_8$ [21–24], as well as the structures and catalytic ability of POSS that are both fully and partially substituted with Ti; that is, $[HTiO_{1.5}]_n$, and $H_8Ti_pSi_{8-p}O_{12}$ [25,26]. In a continuing effort to employ theory to help understand the chemistry of POSS, and possibly design new POSS functionalities, the present work reports the results of calculations on the ability of POSS species to absorb one or more hydrogen molecules. There has been increasing interest in the ability of POSS and related cage compounds to encapsulate small molecules and ions [27–32]. The present analysis of the mechanism of H_2 encapsulation into POSS and metal analogs may have implications with regard to the future development of molecular sieves and H_2 storage. The details of the structure and stability of metal-substituted POSS will be discussed in a separate work [33].

2 Computational methods

The geometries of all molecules of interest have been fully optimized at the Hartree–Fock and second order perturba-

Contribution to the Mark S. Gordon 65th Birthday Festschrift Issue.

Electronic supplementary material The online version of this article (doi:10.1007/s00214-007-0304-8) contains supplementary material, which is available to authorized users.

T. Kudo (✉) · M. Akasaka
Department of Chemistry and Chemical Biology,
Graduate School of Engineering, Gunma University,
Kiryu 376-8515, Japan
e-mail: tkudo@sci.gunma-u.ac.jp

M. S. Gordon (✉)
Department of Chemistry, Iowa State University,
Ames, IA 50011-2030, USA
e-mail: mark@si.fi.ameslab.gov

tion (MP2) [34] levels of theory, using the SBKJC effective core potential [35–37] in order to compare all species considered here at a consistent level of theory. All optimized structures were characterized as minima or transition states by calculating and diagonalizing the corresponding Hessian matrix of energy second derivatives. Single point MP2 energy calculations have been performed at all stationary points to obtain more reliable relative energies. For this purpose, the Zr basis set was augmented by a set of f polarization functions (exponent = 0.300731), in order to provide more reliable relative energies. Likewise, the DZV(d) or DZV(d,p) [38] basis set was used for some of the Ge compounds, while the TZV(d, p) [39,40] basis sets were employed for the Ti and Si compounds. All calculations were performed with the GAMESS electronic structure code [41,42].

3 Results and discussion

3.1 Fully- and partially-substituted metallasilsesquioxanes

Table 1 summarizes the optimized geometries of $[HGeO_{1.5}]_n$ (Ge-T_n) and $[HZrO_{1.5}]_n$(Zr-T_n); $n = 4, 6, 8, 10$ and 12. The analogous structures for the all Si [25,43] and all

Scheme 1

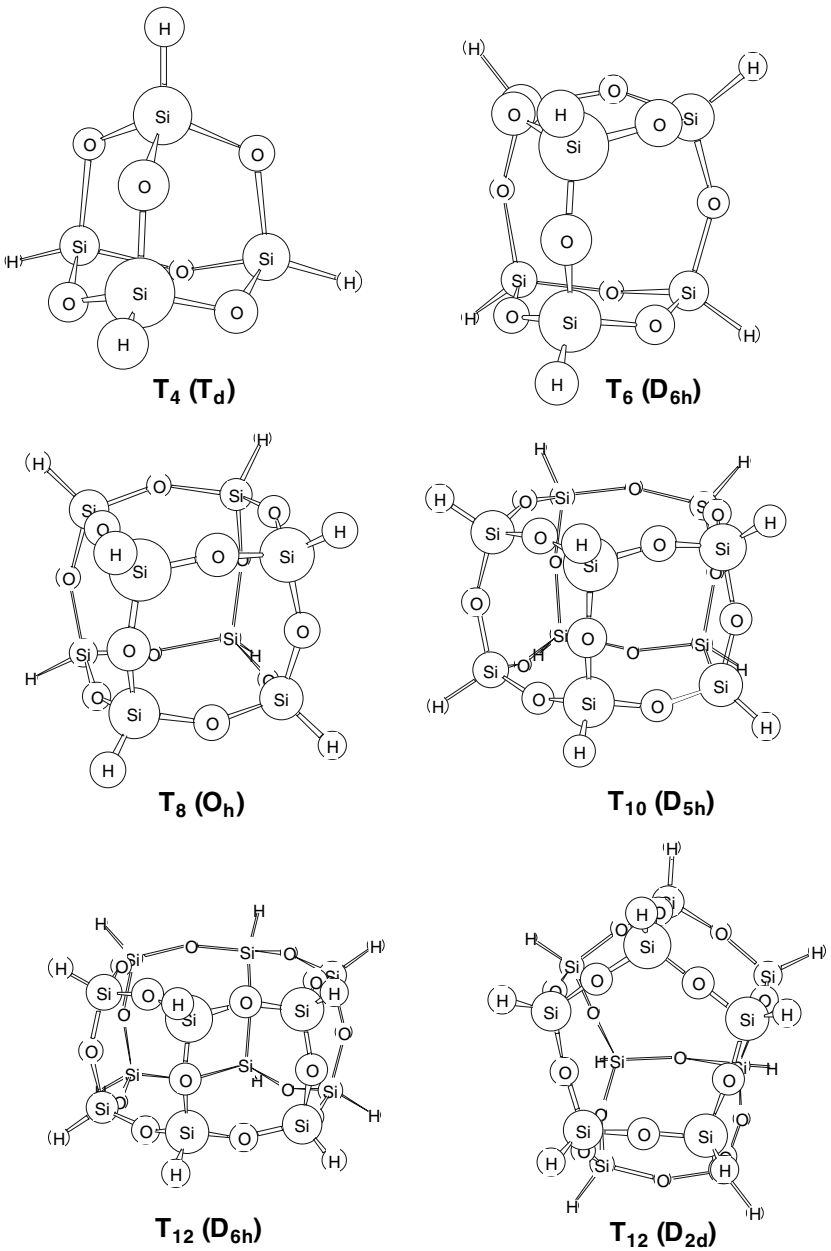

Table 1 MP2/SBK, MP2/DZV(d)[a] and MP2/SBK(f)[b] geometries (Åand degrees) of $[HXO_{1.5}]_n$ (X = Ge and Zr; $n = 4, 6, 8, 10$ and 12)

X		X–O	X–H	X–O–X	O–X–O
Ge					
T_4		(1.798)[a] 1.821	(1.513) 1.512	(115.0) 120.4	(106.6) 103.5
T_6	R_3^c	(1.784) 1.798	(1.515) 1.515	(129.7) 132.2	(109.0) 103.2
	R_4	(1.780) 1.774		(124.7) 145.7	(109.5) 108.6
T_8		(1.770) 1.771	(1.516) 1.516	(144.6) 150.7	(111.3) 108.3
T_{10}	R_4	(1.780) 1.770	(1.525) 1.519	(126.7) 152.0	(110.6) 108.4
	R_5	(1.750) 1.761		(168.6) 157.5	(106.8) 110.0
T_{12}-D_{6h}	R_4	1.771	1.521	151.8	108.5
	R_6	1.759		157.0	110.7
T_{12}-D_{2d}	R_4	1.771	1.519	151.6	108.5
	R_5	1.750		173.4	109.5
Zr					
T_4		< 1.988 >[b] 2.008	< 1.910 > 1.915	< 123.4 > 126.9	< 101.7 > 99.5
T_6	R_3	< 1.983 > 2.000	< 1.900 > 1.908	< 134.2 > 137.4	< 102.8 > 98.9
	R_4	< 1.981 > 1.995		< 144.8 > 151.2	< 107.4 > 106.5
T_8		< 1.980 > 1.992	< 1.897 > 1.905	< 152.5 > 155.0	< 107.4 > 106.0
T_{10}	R_4	< 1.967 > 1.992	< 1.897 > 1.902	< 158.8 > 157.3	< 105.4 > 105.7
	R_5	< 1.968 > 1.994		< 160.3 > 160.4	< 109.9 > 110.2
T_{12}-D_{6h}	R_4	1.972	1.894	161.8	104.3
	R_6	1.976		160.4	114.0
T_{12}-D_{2d}	R_4	1.968	1.895	156.9	97.3
	R_5	1.968		171.6	109.8

[a] The values in parentheses are the MP2/DZV(d) geometries
[b] The values in brackets are the MP2/SBK(f) geometries
[c] R_n means the face into which H_2 inserts

Table 2 Energies (kcal/mol) of the D_{2d} isomer relative to the D_{6h} Isomer of $[HXO_{1.5}]_{12}$ (X = Si, Ti, Ge and Zr) at geometries optimized at various levels of theory

	HF/SBK	MP2/SBK	HF/TZV(d,p)	MP2/TZV(d,p)
Si	−15.3	−11.9	−4.7	−1.1
Ti	−10.8		−6.4[c]	−3.6[c]
Ge	−11.8	−7.7	(−25.6)[a]	
Zr	−12.0 < −8.3 >[b]			

[a] The value in parentheses is the HF/DZV(d) energy
[b] The value in brackets is the HF/SBK(f) energy
[c] Ref. [25]

Ti [25] POSS have been presented previously. Two isomers, the D_{6h} and D_{2d} structures, have been found for the $n = 12$ cage (see Scheme 1). The relative energies of these isomers, together with those of the Si and Ti POSS [25] obtained at various computational levels are shown in Table 2. The D_{2d} structures are more stable in all compounds but the larger basis set significantly stabilizes the D_{6h} structures for Si and Ti-T_{12}. One apparent exception is Ge-T_{12}, for which the D_{2d} structure seems to be the only minimum. The Ge-$T_{12}D_{6h}$ isomer is a minimum at the HF/SBK level of theory, but the MP2/SBK structure has several imaginary frequencies in the range 20–98 cm^{-1}. Also, it is found that the HF/DZV(d) optimized structure has seven imaginary frequencies, suggesting that the D_{6h} isomer of Ge-POSS is not an equilibrium structure. It may be that the larger ring in the Ge compound prefers non planar structures.

The structures and stabilities of all possible Si/Ge mixed T_8, $H_8Ge_pSi_{8-p}O_{12}$ (p = 1 − 7), shown in Scheme 2, were also investigated. The MP2/SBK Si–O bond length and Si–O–Si bond angle in $[HSiO_{1.5}]_8$ ($p = 0$) are 1.700 Åand 152.4°, while the Ge–O distance and Ge–O–Ge angle in $[HGeO_{1.5}]_8$($p = 8$) are 1.771 Å and 150.7°, respectively. In the Si/Ge mixed T_8, there are no significant bond length changes, while the Si–O–Si angle increases slightly (154–155°) and the Ge–O–Ge angle decreases (148 − 150°) in the Ge/Si mixed compounds compared to the all-Si and all-Ge compounds. The Si–O–Ge angle is approximately the average of the original Si–O–Si and Ge–O–Ge angle in all cases (see Scheme 2 and Fig. 1).

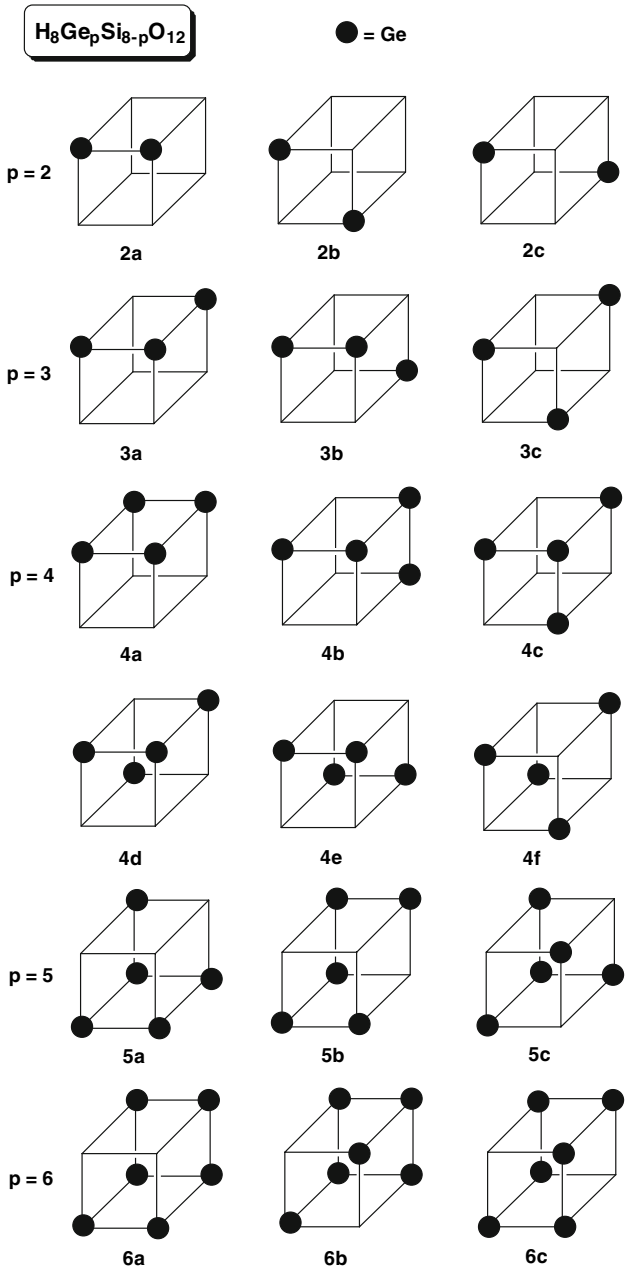

Scheme 2

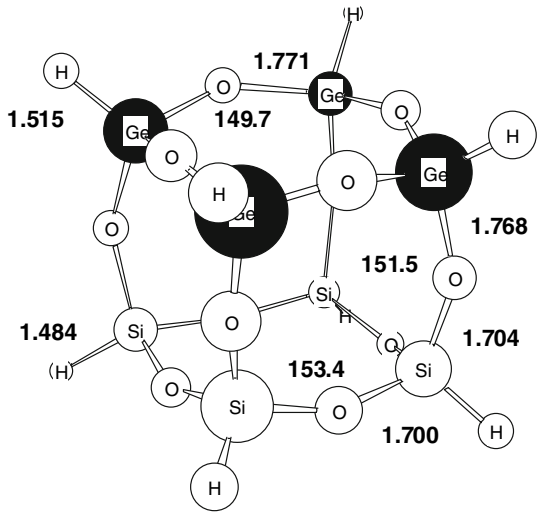

Fig. 1 MP2/SBK optimized structure of $H_8Ge_4Si_4O_{12}$ (4a) in angstroms and degrees

3.2 H_2 insertions

3.2.1 H_2 insertion into silsesquioxanes

The optimized structures of the transition states for H_2 insertion and the corresponding inclusion complexes are displayed in Fig. 2. In the previous computational study of the insertion mechanisms of N_2 and O_2 into POSS, relatively larger cages such as T_8, T_{10} and T_{12}, were considered [27]. Here, the smaller T_6 cage is also considered, because H_2 may be small enough to enter T_6 with smaller barriers than those that were encountered for the larger diatomic molecules. A transition structure for H_2 insertion into the R_3 face of T_6 (see Scheme 3 in which the faces where the H_2 insertion takes place are indicated) was located at the HF/SBK and MP2/SBK levels of theory, with corresponding barrier heights of 212.2 and 177.4 kcal/mol, respectively. However, attempts to find this transition state using HF/TZV(d,p) failed, because the cage opened up. Apparently, the R_3 face is too small even for H_2 to enter. In contrast, insertion through the R_4 face seems to be easier, as the deformation of the ring is relatively small.

As seen from the averaged Si–O distances in Fig. 2, in all transition structures, the ring of the face into which the insertion takes place expands, but the extent of the expansion is very small in the larger cages. In the inclusion complex, the expanded ring of the insertion face shrinks again and the ring sizes of the top and bottom faces are the same. However, the cage that contains the inserted H_2 has clearly expanded compared to the empty cage. For example, the average HF/TZV(d, p) Si–O distance in empty T_6 is 1.633 Å, compared with 1.647 Åfor the inclusion complex at the same level of theory.

For the insertion into the R_6 face of T_{12} (D_{6h}), two types of apparent transition structures were located at both HF/SBK and MP2/SBK levels of theory. In one of these (1) H_2 inserts horizontally (face-on) into the face, while in the second path (2) the insertion reaction takes place vertically (end-on) with a slightly higher energy barrier than (1). However, at these two levels of theory, (2) is found to have three imaginary frequencies and is therefore a third order saddle point, not a transition structure. At the HF/TZV(d,p) level of theory, in contrast, only (2) was located as a transition state with one imaginary frequency, and H_2 maintains its orientation in the inclusion complex. Several attempts were made to find an

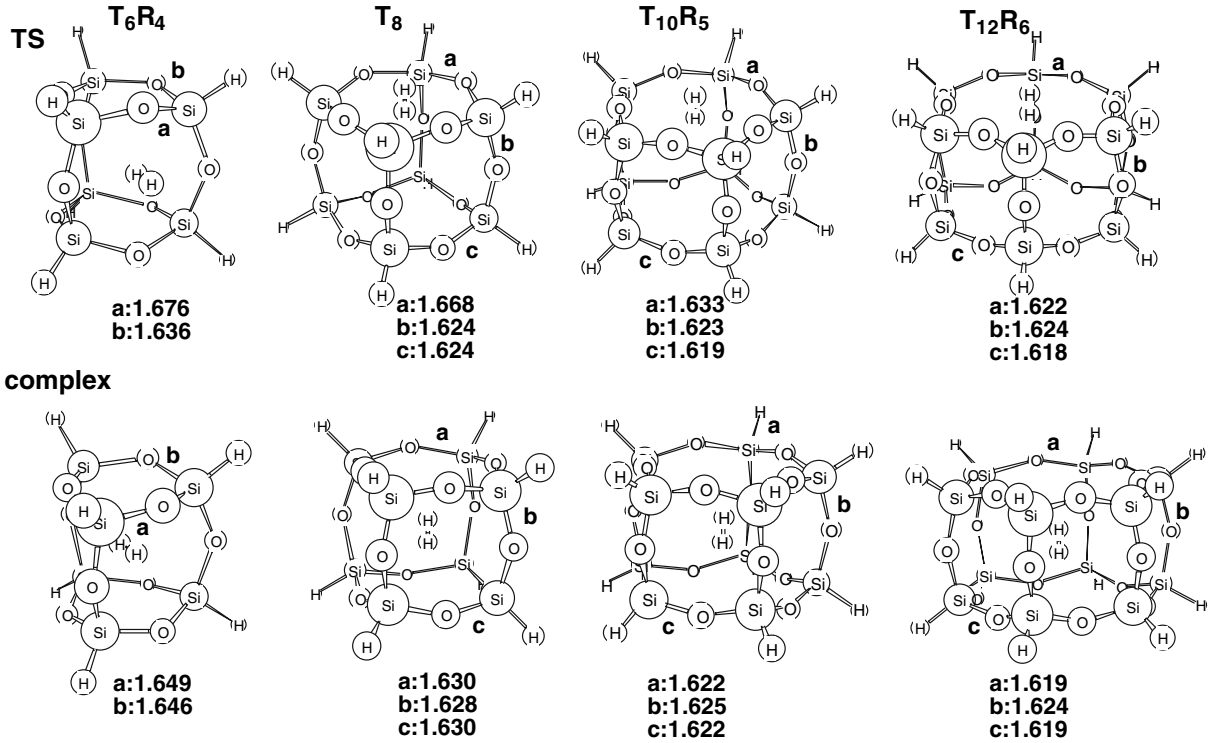

Fig. 2 HF/TZV(d, p) optimized structures of the transition state (upper) and the inclusion complex (lower) for the H_2 insertion into T_n; $n = 6$, 8, 10 and 12 in angstroms. R_n means the face into which the H_2 inserts; for example, T_6 has two kinds of faces or rings (R_3 and R_4) within the cage; T_6R_4 means that the H_2 insertion takes place on the R_4 face of T_6. The three numbers are the averaged distance of Si–O bonds in (*a*) the face where H_2 inserts, (*b*) the side face between the faces in (*a*) and (*b*), (*c*) the opposite face of (*a*)

inclusion complex that directly connects with the face-on TS (1) at the HF/TZV(d,p) level of theory, but no minimum was found. The only structure located that appears to be directly connected with TS (1) has one imaginary frequency corresponding to the transition structure for H_2 rotation inside the cage. The corresponding energy barrier is 1.6 (0.8) kcal/mol at the HF/TZV(d,p) (MP2//HF/TZV(d,p)) level of theory, respectively. It is concluded that the only inclusion complex in T_{12} is the one that corresponds to transition structure (2). Because the R_6 face in T_{12} is large, it could be that the orientation of the H_2 molecule as it enters the cage is not energetically important, even though it appears to enter end-on.

Table 3 summarizes the energies of the insertion transition structure and the inclusion complex relative to the reactant H_2 and empty cages for Si–POSS. The results for the analogous N_2 and O_2 insertions obtained at the same level of theory are also shown for comparison. As expected from the molecular size, the energy barrier for insertion is consistently smallest and the stability of the inclusion complex is largest for H_2. Furthermore, as the size of the cage increases, the energy barrier for insertion decreases.

In the above discussion, all of the insertions are assumed to take place through the face that has the largest ring, as this route is expected to be easier than that through the smaller rings. This is confirmed by the barriers shown in Table 4. More interesting is the observation that the energy barrier depends on the size of the ring where the insertion occurs,

Table 3 MP2/TZV(d,p)//HF/TZV(d,p) energy barriers and net inclusion energies (kcal/mol) relative to reactants for the insertion of H_2, O_2 and N_2 into the largest face of T_n-POSS ($n = 6$, 8, 10 and 12)

	H_2		O_2[a]	N_2[a]
T_6				
TS	75.2	(71.1)[b]		
Complex	46.6	(48.7)		
T_8				
TS	74.7	(72.1)	174.5	188.8
Complex	15.0	(17.1)	82.3	95.0
T_{10}				
TS	24.3	(22.1)	52.6	65.8
Complex	1.4	(3.6)	19.2	24.0
T_{12} (D_{6h})				
TS	6.1	(4.1)	10.4	14.5
Complex	−1.9	(−0.8)	0.3	−1.3

[a] Ref. [27]
[b] The values in parentheses are the MP2/SBK energy barriers

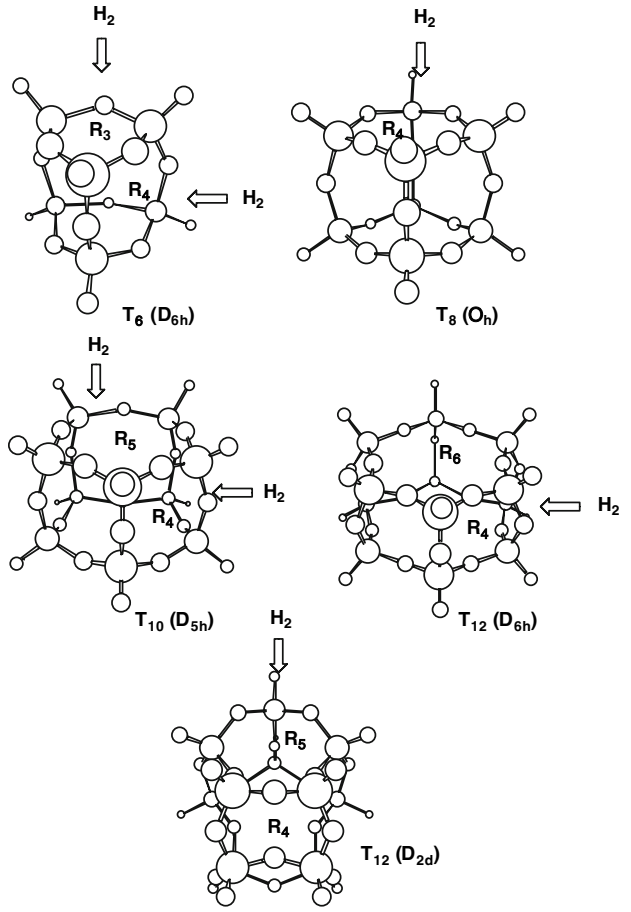

Scheme 3

Table 4 MP2/SBK energy barriers (kcal/mol) for the insertion of H_2 into T_n-POSS ($n = 6$, 8, 10 and 12) through the R_4, R_5 and R_6 faces

	Energy barriers		
	R_4	R_5	R_6
T_6	71.1		
T_8	72.1		
T_{10}	73.1	22.1	
$T_{12}(D_{6h})$	74.3		4.1
$T_{12}(D_{2d})$		22.9	

but does not otherwise depend on the size or shape of the entire cage. That is, the insertion reaction is found to be a local phenomenon.

3.2.2 *H_2 insertion into fully- and partially-substituted metallasilsesquioxanes*

Table 5 summarizes the energetics of the insertion of H_2 into $[HXO_{1.5}]_8$ (fully substituted T_8) and all-*cis* and all-*trans* isomers of $[H(OH)XO]_4$ (fully substituted D_4) ; X = Si, Ge, Ti and Zr. For Si and Ge-D_4, the transition structure of the all-*cis* isomer is lower in energy than that of all-*trans*. This is because a hydrogen-bonding network still exists in the transition structure for the insertion of H_2 into the all-*cis* isomer of the Si and Ge compounds.[1] On the other hand, the energy barrier for the two isomers is about the same for the Ti and Zr analogs in which stabilization by hydrogen-bonding does not exist. The energy barriers for insertion into the cage and ring are similar, since the barrier for insertion into the cage is mirrored by the barrier at the R_4 face. The barriers decrease in the order Si > Ge > Ti > Zr, the same as the order in which the ring and cage size increase. The distances (Å) between the center of the cage (Xc) and metal (X = Si, Ge, Ti, Zr)–r(Xc-X), are 2.862 (X = Si), 2.967 (X = Ge), 3.060 (X = Ti) and 3.369 (X = Zr), respectively. The MP2/SBK energy barrier for Ge-T_{10} is calculated to be 17.3 kcal/mol, much lower than the 57.9 kcal/mol predicted for Ge-T_8. The dependence of the insertion barrier on ring size appears to be a general trend for these species.

Table 5 MP2/SBK energy barriers (kcal/mol) for the insertion of H_2 into all-*cis* and all-*trans* isomers of D_4($[H(OH)XO]_4$) and T_8($[HXO_{1.5}]_8$) (X = Si, Ge, Ti and Zr) and energies (kcal/mol) of inclusion complex relative to the reactants ($T_8 + H_2$)

X	D_4		T_8	
	All-*cis*	All-*trans*	TS	Complex
Si	71.6	75.6	72.1	17.1(−0.05)[a]
Ge	54.8	59.7	57.9	12.6(−0.04)
Ti	44.1	44.0	46.4	8.8(0.17)
Zr	32.2	32.1	32.3	4.6(0.10)

[a] The values in parentheses are the net Mulliken charges on H_2 in the inclusion complexes

The stability of the inclusion complex relative to the separated cage $+H_2$ increases in the order, Si < Ge < Ti < Zr, the same order as the size of the cage. The net charge (Table 5) on H_2 inside the cage is negative for the Si and Ge cages, but the charge is positive for the Ti and Zr cages, suggesting that the direction of charge transfer is opposite in these two groups. Among these compounds, the largest amount of charge transfer is from H_2 to the Ti cage. Most electronegativity scales (e.g., Pauling [44,45]) predict Ge (2.01) > Si (1.90) > Ti (1.54) > Zr (1.33), so the observed charge transfer cannot be explained simply by the relative electronegativities of the metals. In order to determine if the size of the cage plays a role in the magnitude and direction of the charge transfer, an expanded Si-cage with the

[1] Contrary to the fact that two isomers of the Si/Ge-mixed D_4 ring are predicted to be almost planer at the MP2/SBK level, they take significantly non-planar structures at the MP2/DZV(d) level. In the cubic structures, however, each face cannot take a significantly non-planer structure.

Table 6 RVS (reduced variation space) HF/SBK energy decomposition of the interaction energies (kcal/mol) of X-T_8 and H_2 in the Inclusion complex

X	Si	Ge	Ti	Zr
ES	−10.8	−7.8	−6.5	−3.5
EX	37.4	28.1	23.9	13.6
PL	−1.2	−1.0	−1.8	−1.0
CT	−2.1	−1.8	−1.3	−0.9
MIX	−0.6	−0.4	−0.4	−0.3
Total	22.7	17.1	13.9	7.9

Table 7 Energy barriers (kcal/mol) for the insertion of H_2 into $H_8Ge_pSi_{4-p}O_4$ ($p = 0-4$) at the HF/SBK, MP2/SBK and MP2/DZV(d, p)//MP2/SBK[a] levels of theory

p	Isomer	Energy barriers	
		HF/SBK	MP2/SBK
0		82.2	68.5(72.9)[a]
1		78.0	64.7(65.3)
2	A[b]	74.0	61.2(58.2)
	B[b]	74.1	61.3(58.5)
3		70.4	58.0(52.6)
4		66.9	55.0(48.0)

[a] The values in parentheses are the MP2/DZV(d, p)//MP2/SBK values
[b] A is the isomer with nearest neighbor Ge and Si atoms while B is an isomer with alternating Ge and Si (See Fig. 3)

same size as the Zr-inclusion complex was examined. This cage expansion alters the net charge on H_2 from negative to slightly positive (0.004). Therefore, the size of the cage seems to affect the direction of charge transfer. Furthermore, an RVS (reduced variation space) energy decomposition analysis [46] was employed (see Table 6) to investigate the interaction energies in the inclusion complexes in more detail. Since the MIX term is very small, the well-defined terms in the RVS analysis are meaningful. The exchange repulsion (EX) clearly is the primary source of the destabilization of the inclusion complex, while the main contributor to stability of the complexes is the electrostatic term, ES. The other two contributors to the interaction energy, the polarization (POL) and charge transfer (CT) terms are small. Both EX and ES decrease in the order Si > Ge > Ti > Zr.

Next, consider the H_2 insertion into Si–D_4 and Si–T_8 partially substituted with Ge. The transition structures and the energy barriers for the insertion into the Si/Ge-mixed-D_4–$H_8Ge_pSi_{4-p}O_4$; $p = 0-4$, are shown in Fig. 3 and Table 7, respectively. As the figure shows, H_2 inserts through the center of the R_4 face for $p = 0$, 2 with alternating Ge and Si (isomer B), and 4, while in the other cases the H_2 position is closer to the Ge atoms than the Si atoms, probably because of

Table 8 HF/SBK and MP2/SBK[a] energies (kcal/mol) for the H_2 insertion transition states into Ge/Si-T_8, $H_8Ge_4Si_4O_{12}$, and the inclusion complex relative to the reactants ($H_8Ge_4Si_4O_{12} + H_2$)

p	Isomer[b]	Face[b]	TS	Complex
4	a	1	86.9(72.5)[a]	20.2(14.6)
		2	70.4(57.7)	Same as 1
		3	78.0(64.5)	20.1(14.6)
	b	1	78.0(64.5)	20.2(14.7)
		2	74.1(61.0)	20.2(14.7)
		3	82.3(68.4)	Same as 2
	c	1	74.1(61.0)	20.2(14.6)
		2	82.3(68.4)	Same as 1
	d	1	74.1(61.0)	20.2(14.7)
		2	82.3(68.4)	same as 1
		3	78.0(64.5)	20.2(14.7)
		4	78.2(64.7)	Same as 3
	e	1	78.2(64.6)	20.2(14.8)
		2	78.1(64.6)	20.3(14.8)
	f		78.1(64.7)	20.2(14.7)

[a] The values in parentheses are the MP2/SBK//MP2/SBK values
[b] See Scheme 4

available space. This larger space makes the insertion reaction easier as seen from the energy barriers in Table 7.

For the H_2 insertions into the equally mixed Si/Ge T_8, $H_8Ge_4Si_4O_{12}$, all possible routes into the six isomers (see Scheme 4 and Table 8) were investigated. In Scheme 4, the arrows with numbers indicate the direction (face) from which the H_2 molecule is approaching. The corresponding barriers are listed in Table 8.

Shown in Fig. 4 are the optimized structures of the three types of transition structure for the H_2 insertion into isomer (4a) of $H_8Ge_4Si_4O_{12}$ and the two kinds of inclusion isomers that were found. For each transition structure, the geometry change in the cage is only seen at the face (Si_4, Ge_4, or Si_2Ge_2) into which H_2 inserts, suggesting this is a local phenomenon, as was noted for the per-Si–POSS compounds. The cage in the inclusion compounds seems to expand compared to the empty cage. As for the fully substituted T_8 species, there is a strong correlation between the energy barriers for the D_4 rings and those for the T_8 compounds in which the insertion occurs into the analogous face. The insertion into the cage seems to need a slightly larger energy, due to geometric constraints in the cage. However, the stability of the inclusion complex (Table 8) is apparently unrelated to the isomer or the face through which H_2 inserts. For the mixed $p = 1$ and $p = 2$ Si/Ge-T_8 compounds (Table 9), the stability of the inclusion complex depends only on the number of Ge or Si atoms in T_8 and increases as the number of Ge atoms increases, due to the increasing size of the cage.

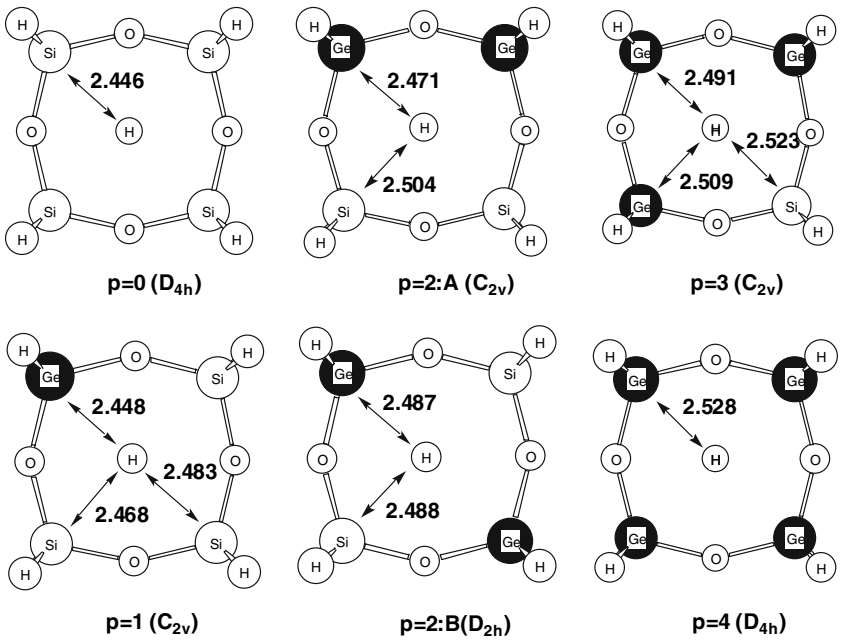

Fig. 3 MP2/SBK optimized structures of the transition state for the H_2 insertion into $H_8Ge_pSi_{4-p}O_4$; $p = 0 - 4$ in angstroms

Scheme 4

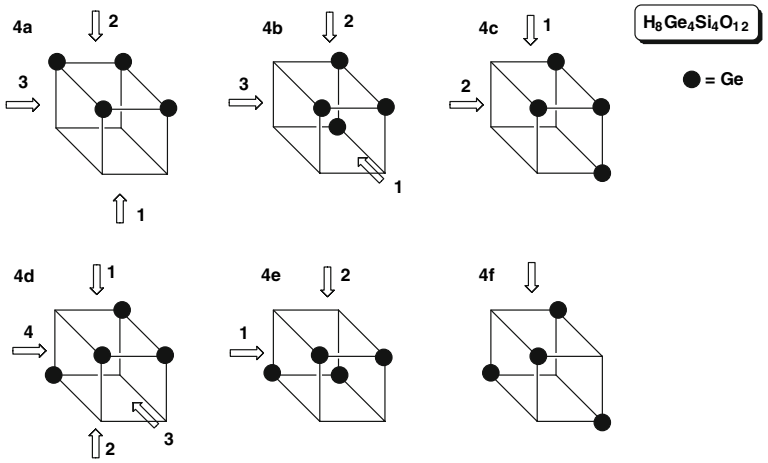

3.2.3 Insertion of two H_2 molecules into metallasilsesquioxanes

Now, consider the insertion of *two* H_2 molecules into the larger POSS compounds (T_{10} and T_{12}) and Ge-POSS (Ge-T_{10}). The optimized structures for the transition states for inserting the second H_2 and the corresponding inclusion complexes are shown in Fig. 5. In all POSS considered here, the second H_2 inserts vertically (end-on) into the face plane as was found for the first H_2, and the two H_2 molecules lie along a line (collinear) inside the cages.[2] The second H_2 has a tendency to push the first H_2 toward one of the faces of the cage. No inclusion complex consisting of T_{12} and two H_2 molecules were found, even though the corresponding transition state ($T_{12}R_6$-$2H_2$-TS in Fig. 5) was found. The IRC from this TS leads to the T_{12}-$1H_2$ -complex and one free H_2, suggesting that the second H_2 forces the first H_2 out of the cage. Another T_{12}-$2H_2$ complex was found, in which the two H_2 molecules sit parallel to each other. However, this complex is higher in energy than the $T_{12}R_6$-$2H_2$-TS transition state and has one imaginary frequency. A search was initiated to find a minimum by following the mode corresponding to the imaginary frequency, but the resultant structure is the $T_{12}R_6$-$2H_2$-TS.

The potential energy surfaces for the first and second H_2 insertion reactions are displayed in Figs. 6 and 7, respectively. As the figures show, the inclusion of the second H_2 requires a very high energy and significantly decreases the stability relative to the single H_2 inclusion complex. The complex

[2] We have located a different transition structure for the H_2 insertion into Ge-T_8 at the MP2/SBK level. In the structure, the second H_2 inserts from the side face of the first inclusion complex so two H_2 molecules form T-shaped structure inside the cage. The energy barrier is calculated to be 74.4 kcal/mol. For the resultant inclusion complex (68.5 kcal/mol above the reactants, Ge-T_8 and two isolated H_2), however, two H_2 molecules align on one line like in other cases.

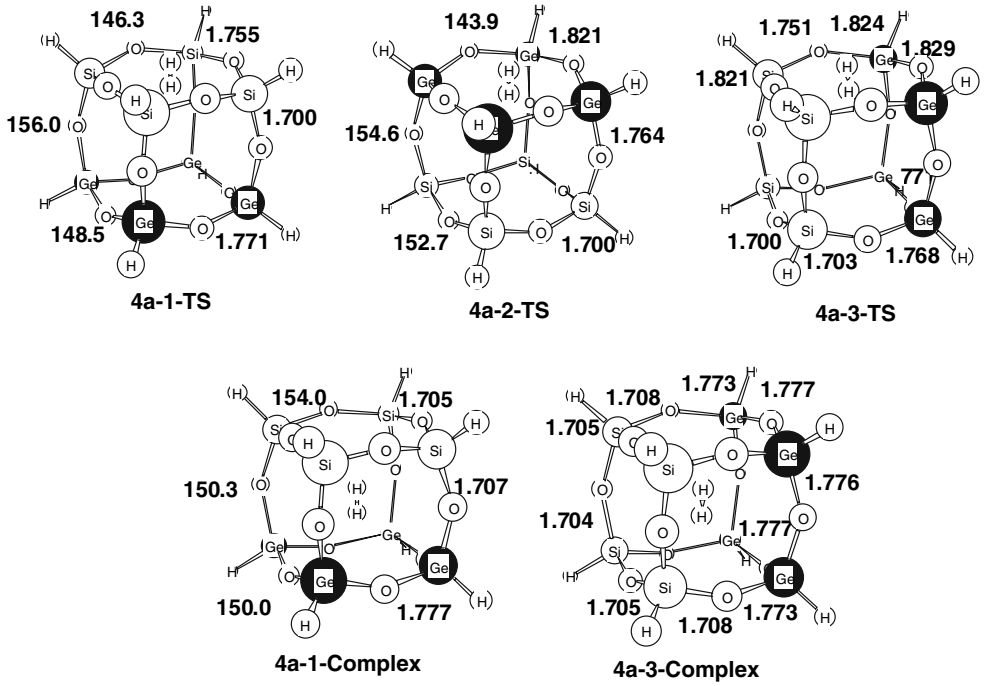

Fig. 4 MP2/SBK optimized structures of the transition states (*upper*) and the inclusion complexes (*lower*) for the two H_2 insertions into isomer a of $H_8Ge_4Si_4O_{12}$ (4a) in angstroms

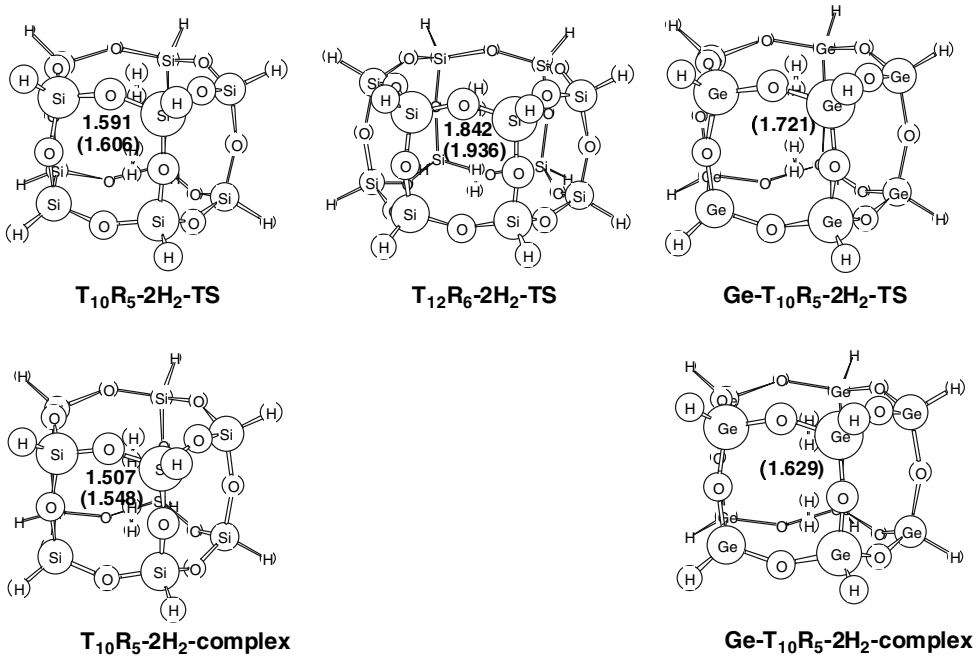

Fig. 5 HF/TZV(d,p) optimized structures of the transition state and the inclusion complex for the two H_2 insertion into T_{10}, T_{12} and Ge-T_{10} in angstroms. The numbers are the distance between each H_2 molecule. The values in *parentheses* are the MP2/SBK distances

with 2 H_2 may be too unstable to exist for Si and Ge-T_{10}, and for Si-T_{12} the second H_2 seems to push out the first H_2, even though there seems to be sufficient room for the two H_2 molecules. This probably occurs because of the low energy barriers for H_2 molecules passing through the T_{12} cage.

4 Concluding remarks

The H_2 insertion reactions for various sizes of POSS, as well as their Ti, Ge and Zr analogs and the Si/Ge-mixed POSS were investigated. The structures of Ge-POSS, Ti-POSS and

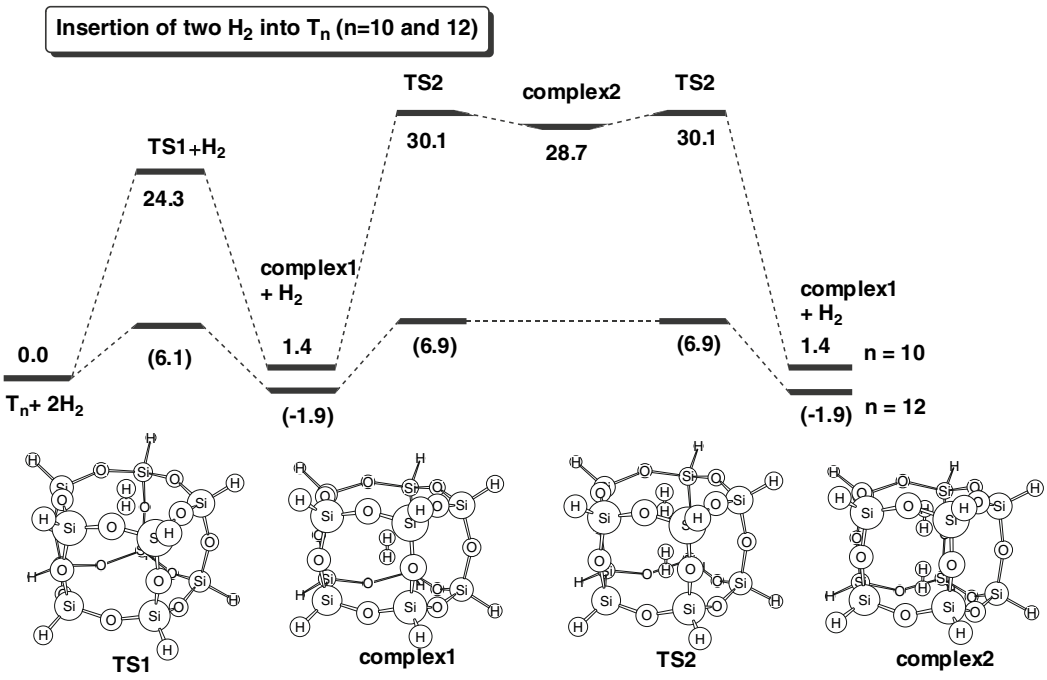

Fig. 6 MP2/TZV(d,p) potential energy surface (kcal/mol) for the H_2 insertion into T_{10} and T_{12} based on the HF/TZV(d,p) optimized geometries. The values in the *parentheses* are for T_{12}

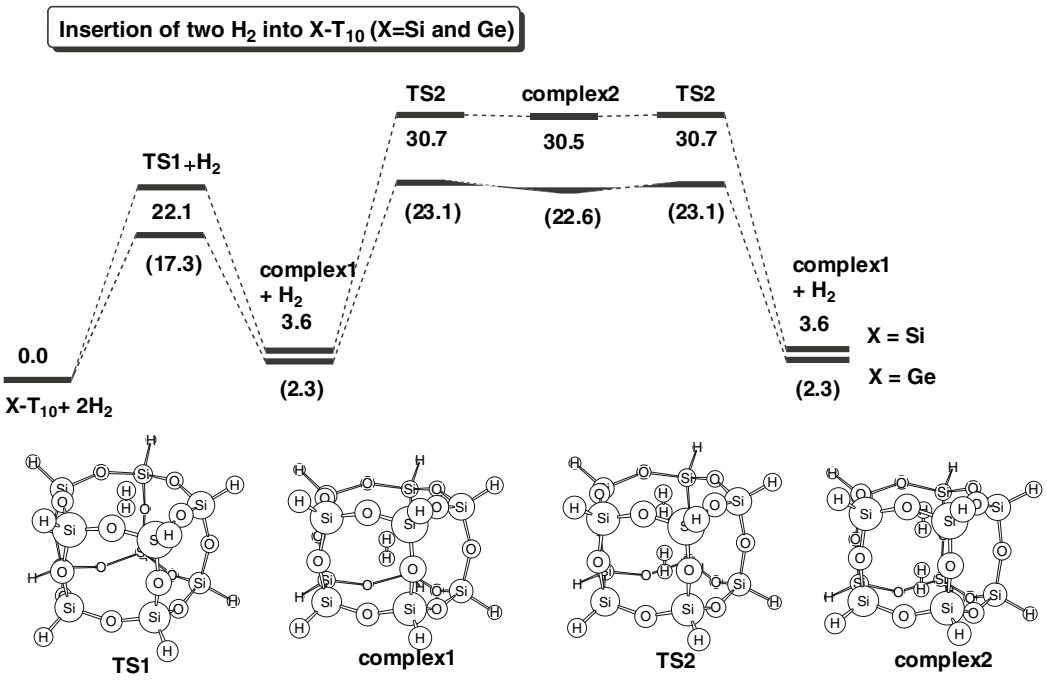

Fig. 7 MP2/SBK potential energy surface (kcal/mol) for the H_2 insertion into T_{10} and Ge-T_{10} based on the MP2/SBK optimized geometries. The values in the *parentheses* are for Ge-T_{10}

Zr-POSS are similar to those of Si-POSS, and the relative stabilities of the two isomers of the largest (T_{12}) cage are also same in all substituted compounds. For the Si/Ge-mixed POSS, geometrical changes are observed only in the regions at which Ge substitution has taken place, while the other regions undergo little change.

Table 9 HF/SBK and MP2/SBK[a] energies (kcal/mol) of inclusion complexes relative to the reactants ($H_8Ge_pSi_{8-}pO_{12}+H_2$; $p = 0, 1, 2$ and 8)

p	Isomer	Face	Complex
0			23.3(17.1)[a]
1			22.5(16.5)
2	a	1	21.7(15.8)
		2	21.7(15.9)
	b	1	21.7(15.9)
		2	21.7(15.9)
	c		21.7(15.9)
8			17.5(12.6)

[a] The values in parentheses are the MP2/SBK//MP2/SBK values

As expected, the H_2 insertion barrier decreases as the ring size increases, regardless of which metal is used to form the POSS. Among Si-, Ge-, Ti- and Zr-T_8, the Zr compound has the largest (most open) cage structure, so the H_2 insertion is predicted to be easiest (lowest barrier) for this species. With regard to synthetic considerations, the combination of a relatively small barrier ($\sim$ 32 kcal/mol) and small endothermicity ($\sim$ 4.5 kcal/mol) would suggest that the Zr-T_8 POSS is the most likely target, followed by the Ti-T_8 POSS. However, a firmer conclusion will require higher levels of theory, as well as dynamics studies.

With regard to all Si POSS, the barrier and the endothermicity decrease as the size of the cage and the insertion face increase. Insertion into the T_{10} cage is almost thermal neutral and has a 24.3 kcal/mol barrier, so this species may be a viable synthetic target.

Importantly, the energy barrier depends on the size of the ring through the insertion occurs, but does not depend on the size or shape of the entire cage. In the largest cage (T_{12}), H_2 is expected to move around inside the cage and pass through the cage with little energy cost.

The insertion of two H_2 molecules is predicted to be difficult, due to high energy barriers in the smaller cages and the ease with which one H_2 can force the other out of the cage for the larger (e.g., T_{12}) cages.

Acknowledgement This work has been supported by the Project on Development of Silicon-Based Functional Materials (T. Kudo) and the Air Force Office of Scientific Research (M. S. Gordon). Computer time has been made available via a Grand Challenge grant from the DOD High Performance Computing Modernization Office on the T3E computers at ERDC and AHPCRC.

References

1. Voronkov MG, Lavrent'yev VL (1982) Top Curr Chem 102:199
2. Feher FJ, Newman DA, Walzer JF (1989) J Am Chem Soc 1111:1741
3. Baney RH, Itoh M, Sakakibara A, Suzuki T (1995) Chem Rev 95:1409
4. Feher FJ, Budzichowski TA (1995) Polyhedron 14:3239
5. Choi J, Harcup J, Yee AF, Zhu Q, Laine RM (2001) J Am Chem Soc 123:11420
6. Tamaki R, Tanaka Y, Asucion MZ, Choi J, Laine RM (2001) J Am Chem Soc 123:12416
7. Franco R, Kandalam AK, Pandey R, Pernisz UC (2002) J Phys Chem B 106:1709
8. Lin T, He C, Xiao Y (2003) J Phys Chem B 107:13788
9. Chen Y, Schneider KS, Banaszak Holl MM, Orr BG (2004) Phys Rev B 70:85402
10. Adachi K, Tamaki R, Cyujo Y (2004) Bull Chem Soc Jpn 77:2115
11. Hillson SD, Smith R, Zeldin M, Parish CA (2005) J Phys Chem A 109:8371
12. Striolo A, McCabe C, Cummings PT (2005) Macromolecules 38:8950
13. Ionescu TC, Qi F, McCabe C, Striolo A, Kieffer J, Cummings PT (2006) J Phys Chem B 110:2502
14. Edelmann FT, Giebmann S, Fischer A (2001) J Organomet Chem 620:80
15. Lorenz V, Spoida M, Fischer A, Edelmann FT (2001) J Organomet Chem 625:1
16. Murugavel R, Shete VS, Baheti K, Davis P (2001) J Organomet Chem 625:195
17. Fei Z, Busse S, Edelmann FT (2002) J Chem Soc Dalton Trans 2587
18. Gerritsen G, Duchateau R, Van Santen RA, Yap GPA (2003) Organometallics 22:100
19. Lorenz V, Giebmann S, Gun'ko YK, Fischer AK, Gilje JW, Edelmann FT (2004) Angew Chem Int Ed 43:4603
20. Pescarmona PP, Vander Waal JC, Maschemeyer T (2004) Chem Eur J 10:1657
21. Kudo T, Gordon MS (1998) J Am Chem Soc 120:11432
22. Kudo T, Gordon MS (2000) J Phys Chem A 104:4058
23. Kudo T, Gordon MS (2002) J Phys Chem A 106:11347
24. Kudo T, Machida K, Gordon MS (2005) J Phys Chem A 109:5424
25. Kudo T, Gordon MS (2001) J Phys Chem A 105:11276
26. Kudo T, Gordon MS (2003) J Phys Chem A 107:8756
27. Tejerina B, Gordon MS (2002) J Phys Chem B 106:11764
28. Villaescusa LA, Lightfoot P, Morris RE (2002) Chem Commun 2220
29. Bassindale AR, Pourny M, Taylor PG, Hursthouse MB, Light ME (2003) Angew Chem Int Ed 42:3488
30. Park SS, Xiao C, Hagelberg F, Hossain D, Pittman CU Jr, Saebo S (2004) J Phys Chem A 108:11260
31. Satre G, Pulido A, Corma A (2005) Chem Commun 2357
32. Pach M, Macrae RM, Carmichael I (2006) J Am Chem Soc 128:6111
33. Kudo T, Akasaka M, Gordon MS (to be prepared)
34. Pople JA, Seeger R, Krishnann R (1979) Int J Quantum Chem S 11:149
35. Stevens WJ, Basch H, Krauss M (1984) J Chem Phys 81:6026
36. Stevens WJ, Krauss M, Jasien P (1992) Can J Chem 70:612
37. Cundari T. R., Stevens W. J. (1993) J Chem Phys 98:5555
38. Binning RCJr, Curtiss LA (1990) J Comput Chem 11:1206
39. Wachters AJH (1970) J Chem Phys 52:1033
40. Rappe AK, Smedley TA, Goddard WAIII (1981) J Phys Chem 85:2607
41. Schmidt MW, Baldridge KK, Boatz JA, Elbert ST, Gordon MS, Jensen JH, Koseki S, Matsunaga N, Nguyen KA, Su S, Windus TL, Dupuis M, Montgomery JAJr (1993) J Comput Chem 14:1347
42. Gordon MS, Schmidt MW (2005) In: Dykstra CE, Frenking G, Kim KS, Scuseria GE (eds) Advances in Electronic Structure Theory: GAMESS a Decade Later, Theory and Applications of Computational Chemistry, Chap. 41. Elsevier, Amsterdam

43. Earley CW (1994) J Phys Chem 98:8693
44. Pauling L (1960) The nature of chemical bond, 3rd edn. Cornell University Press, Ithaca p 93
45. Allred AL (1961) J Inorg Nucl Chem 17:215
46. Stevens WJ, Fink WH (1987) Chem Phys Lett 139:15